

Article

Effect of Initial Microstructure on the Temperature Dependence of the Flow Stress and Deformation Microstructure under Uniaxial Compression of Ti-407

Luis Barboza ^{1,*}, Enrique López ¹, Hugo Guajardo ¹ and Armando Salinas ^{2,*} 

¹ Facultad de Ingeniería Mecánica y Eléctrica, Universidad Autónoma de Nuevo León, San Nicolás de los Garza, Nuevo León 66455, Mexico; enrique.lopezcl@uanl.edu.mx (E.L.); hugo.guajardog@uanl.edu.mx (H.G.)

² Centro de Investigación y Estudios Avanzados del IPN, Ramos Arizpe, Coahuila 25900, Mexico

* Correspondence: luis.barbozagn@uanl.edu.mx (L.B.); armando.salinas@cinvestav.edu.mx (A.S.); Tel.: +52-811-760-9774 (L.B.); +52-844-438-9600 (ext. 8649) (A.S.)

Abstract: In this study, the influence of initial microstructure and deformation temperature on the flow stress behavior and microstructural evolution of TIMETAL[®] 407 (Ti-407) alloy are investigated. For this purpose, compression cylinders were β -annealed at 940 °C and then cooled to room temperature using furnace cooling, static air, and water quenching to promote three initial microstructures with different α lath thicknesses. The annealed cylinders were compressed isothermally in the range of 750 °C to 910 °C at a constant crosshead speed of 0.05 mm/s up to an engineering strain of -0.8 . The resulting stress–strain curves are discussed in terms of the morphology and distribution of the α and β phases. It was found that flow stress is inversely proportional to deformation temperature for all initial microstructures. At the lowest temperatures, compressive yield strength was higher in water-quenched and air-cooled samples than in furnace-cooled specimens, suggesting that the acicular α -phase morphology obtained by rapid cooling could enhance mechanical strength by hindering dislocation motion. Two high-temperature flow regimes were determined based on the shape of the flow stress curves, indicating microstructural changes occurring during deformation. At higher temperatures, the effect of the initial microstructure is negligible as the primary α phase is transformed to the β phase at around 850 °C irrespective of the initial α -lath thickness.

Keywords: Ti-407; uniaxial compression; microstructural evolution; β anneal



Citation: Barboza, L.; López, E.; Guajardo, H.; Salinas, A. Effect of Initial Microstructure on the Temperature Dependence of the Flow Stress and Deformation Microstructure under Uniaxial Compression of Ti-407. *Metals* **2024**, *14*, 505. <https://doi.org/10.3390/met14050505>

Academic Editor: Andrey Belyakov

Received: 28 February 2024

Revised: 15 April 2024

Accepted: 18 April 2024

Published: 26 April 2024



Copyright: © 2024 by the authors. Licensee MDPI, Basel, Switzerland. This article is an open access article distributed under the terms and conditions of the Creative Commons Attribution (CC BY) license (<https://creativecommons.org/licenses/by/4.0/>).

1. Introduction

Titanium alloys are widely used in aerospace, power generation, chemical processing, and marine applications due to their high specific strength, good thermal stability, and excellent corrosion resistance, despite their high buy-to-fly ratio and associated forging and machining difficulties. This has led to a strong drive for near-net titanium fabrication [1] as well as the development of titanium alloys with lower associated manufacturing costs.

Titanium alloy TIMETAL[®] 407, or Ti-407 (Ti-4V-0.8Al-0.08Fe-0.2Si, in wt.%), is an ($\alpha + \beta$) alloy developed by TIMET as a lower cost direct replacement of Ti-6Al-4V alloy, the most commonly used titanium alloy worldwide [2]. Ti-407 may be used with advantage for applications where energy absorption during fracture and High Cycle Fatigue (HCF) endurance limit are the key design criteria [3], such as engine fans and compressor casings. In terms of fabrication, Ti-407 alloy was designed for improved manufacturability, including low-temperature forming and increased machining speeds.

One of the main benefits and most important features offered by Ti-407, compared with Ti-6Al-4V, is a significant improvement in ductility, offering superior manufacturability and increased machining speeds with lower contact forces. In terms of thermomechanical processing, the lower flow stress, greater malleability, and wider process window of Ti-407

should allow it to be forged using a lower quantity of reheats while exhibiting less surface cracking and requiring less machining.

In regard to its performance in service, due to its relatively low strength, Ti-407 may not be able to substitute all Ti-6Al-4V components, but promisingly, Ti-407 demonstration casings have shown 2.5 times the lateral expansion and more than twice the impact energy was absorbed compared to Ti-6Al-4V [4]. In tension, Ti-407 alloy has significantly increased ductility (quasi-static strain to failure increase of 60%) but reduced strength (quasi-static ultimate strength reduction of 34%) in comparison to Ti-6Al-4V. The combination of an increase in ductility and a reduction in strength gives similar toughness values for the two alloys [5].

Ti-407 alloy was designed by starting with the same vanadium content as Ti-6Al-4V to retain the β phase at room temperature, but with lower aluminum (~0.8 wt.%). Reducing Al content improves ductility [6] and machinability of titanium alloys [7], β -eutectoid elements like Si and Fe are also added to provide some solid solution strengthening [8]. Although Ti-407 has a similar amount of β stabilizers, its density is higher when compared to Ti-6Al-4V, due to the overall reduction in aluminum content. However, with an appropriate component design, Ti-407 could be incorporated as a weight-neutral, alternative alloy [9]. In terms of its β -transus temperature ($T_{\beta t}$), the temperature at which the alloy is constituted by 100% β phase, it is expected to be significantly lower than that of Ti-6Al-4V due to the aluminum reduction, as described in the titanium–aluminum binary diagram [10]. The $T_{\beta t}$ has been reported as high as 890 °C by the alloy supplier. However, recently, Singh and Souza reported $T_{\beta t} = 875$ °C [11].

Regarding the effect of ($\alpha + \beta$) processing on room-temperature mechanical properties, it has been reported that the toughness of Ti-407 alloy after solution and aging treatments (STAs) is significantly improved using oil quenching rather than air cooling or water quenching after the solution treatment. Samples tested under uniaxial compression at room temperature exhibited a higher strain to fracture [12], indicating that the cooling rate from the ($\alpha + \beta$) field influences the room-temperature flow stress behavior.

From the manufacturing standpoint, the effect of multi-pass high-temperature rolling and subsequent annealing on the extent of spheroidization of the α phase as well as the texture development has been assessed, and it has been reported that high stored energy prior to annealing and the activation of deformation twinning when samples were deformed at 650 °C and rolled to 75% reduction resulted in greater spheroidization of primary α phase and transformed β phase [8]. While these findings shed light on the microstructural development of Ti-407 alloy, the interaction of the lamellar microstructure typically present in the initial steps of the forging process with the deformation temperature and its effects on the flow stress behavior remain unclear.

Microstructural evolution in titanium alloys has been broadly studied [13–15], recently including the incorporation of mathematical modeling, computational simulation [16,17], and machine learning algorithms [18] that can predict phase diagrams, material properties, crystal structures [19], martensite formation [20], and β -transus temperature [21] to a certain extent based on existing materials databases, which rely heavily on the accumulated literature [22]. Nevertheless, the addition of multiple elements to new titanium alloys may cause more phases to form, making available a wide variety of microstructures, especially for engine components obtained through a long thermomechanical processing route [23]. Therefore, the characterization of newly introduced titanium alloys in terms of microstructural manipulation via thermomechanical processing is still of paramount importance.

The objective of this study is to characterize the hot deformation behavior of Ti-407 in uniaxial compression, as it is the dominant deformation mode in forging [24], over a wide range of temperatures with different initial lamellar microstructures varying in α -lath thickness. The results of this work allow correlating high-temperature flow stress with microstructural evolution in terms of α -phase globularization for the optimization of sub- and super- β -transus forging processes, typically used in the manufacture of large titanium alloy components.

2. Materials and Methods

Ti-407 material was supplied in the form of a seamless rolled ring processed with a combination of temperatures above and below the β transus ($T_{\beta t}$), that is, in the β -phase field and in the $(\alpha + \beta)$ temperature region, respectively. $T_{\beta t}$ was determined by non-isothermal dilatometry, as this technique is an effective method for studying the phase transformation process [25,26] since the expansion curve and its first derivative can indicate the onset, development, and completion of the phase transformation [27]. The thermal dilatometry test was performed using a Linseis model L75 vertical dilatometer at a constant heating rate of 5 °C/min from room temperature to 900 °C. The thermal expansion of a cylindrical sample measuring 10 mm in diameter and 30 mm in length was plotted as a function of temperature, and its first derivative with respect to time was obtained to indicate the rate of expansion. The chemical composition of the as-received material is listed in Table 1.

Table 1. Chemical composition of the as-received Ti-407 material, in wt.%.

V	Al	Si	Fe	O	C	N	Ti
3.6	0.85	0.21	0.26	0.15	<0.03	<0.008	Bal.

Once the $T_{\beta t}$ was determined, a set of compression cylinders measuring 10 mm in diameter and 15 mm in height were machined to have their axes parallel to the axial direction of the rolled ring. To reset the microstructure of the incoming material, the machined cylinders were β -annealed at 940 °C for one hour using a resistance-heated muffle furnace and then cooled to room temperature in water, still air, or within the furnace to promote the formation of different lamellar α -phase morphologies. It is noteworthy that the cooling rate after solution treatments is considered the principal and most critical processing variable that affects the nucleation mechanism and the kinetics of the $\beta \rightarrow \alpha$ phase transformation, as the content of grain boundary α (α_{GB}), α colony size, and lamellar α thickness all decrease with an increase in the cooling rate [28].

The β -annealed cylinders were then isothermally deformed in uniaxial compression using an MTS (Materials Testing System) universal testing machine model QTest, at a constant crosshead speed of 0.05 mm/s (initial strain rate $\dot{\epsilon} \approx 5 \times 10^{-3} \text{ s}^{-1}$) to reach an effective strain of -0.8 under an inert atmosphere of argon to minimize oxidation; the isothermal deformation temperatures were 750 °C, 770 °C, 790 °C, 810 °C, 830 °C, 850 °C, 870 °C, 890 °C, and 910 °C. The samples were heated to the defined temperatures for 30 min before being compressed; colloidal graphite was used as a lubricant to reduce friction between the Ti-407 samples and the compression anvils. Upon reaching the target strain, the deformed cylinders were air-cooled to room temperature. Stress–strain curves were constructed with load and displacement data obtained from the universal testing machine for every deformation temperature and initial microstructure combination.

After compression testing, the deformed cylinders were sectioned parallel to the compression axis, and their cross-section microstructure was characterized by means of optical microscopy using a Zeiss microscope model Axio Observer. The samples were ground with silicon carbide sandpapers to 1200 grit and then mechanically polished using a diamond paste solution, followed by chemical etching in a 2 mL HF + 4 mL HNO₃ + 100 mL water solution; α - and β -phase morphologies and distributions were characterized using a JEOL JSM-IT200 scanning electron microscope.

The globular α fraction (%) and the α lath thickness were determined from scanning electron microscope images using ImageJ software (Version 1.53k), based on the relative content of globular α in the SEM images. In the present work, α platelets with an aspect ratio (length-to-thickness) < 3 are considered as globular. The value of 3 was selected based on other studies performed on $\alpha + \beta$ titanium alloys [8,29].

3. Results and Discussion

The dilatometric curve of the phase transformation from $\alpha \rightarrow \alpha + \beta \rightarrow \beta$ on heating is shown in Figure 1. Tangential lines (black lines) have been added to the expansion curve (red curve) to facilitate visualization of the non-linear expansion behavior during the $\alpha + \beta \rightarrow \beta$ transformation. The first derivative of the expansion with respect to time (blue curve) was included to assess the peak of the $\alpha + \beta \rightarrow \beta$ transformation. The onset, peak, and completion of the $\alpha + \beta \rightarrow \beta$ transformation were identified at 796 °C, 839 °C, and 869 °C, respectively. Since titanium has a high solubility of oxygen in both α and β phases, oxygen present in the atmosphere diffuses into the sample during the dilatometric tests, and with this increase in oxygen content, $T_{\beta t}$ also increases [30]. Under these conditions, $T_{\beta t}$ was approximately 869 °C. This value is within 1% of that reported by Singh and Souza [11].

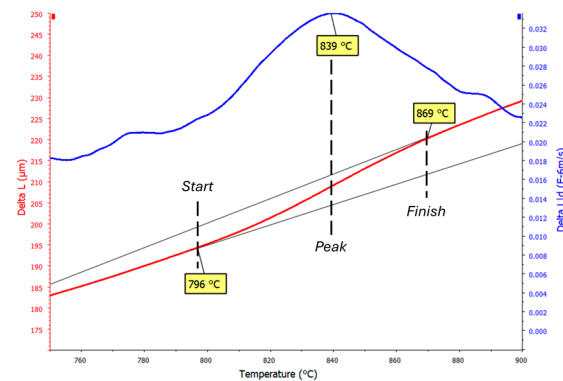


Figure 1. Dilatometric curve during heating process at a constant heating rate of 5 °C/min.

Figure 2 shows SEM secondary electron images corresponding to the three initial conditions of Ti-407 alloy after β annealing and subsequent cooling; these images consist primarily of prior β -grain boundaries and intragranular α laths which exhibit a decrease in thickness as the cooling rate increased. It must be noted that the cooling rate increases from Figure 2a–c. The different phases found were determined based on their appearance and were identified using a commonly accepted nomenclature for titanium alloy microconstituents [31].

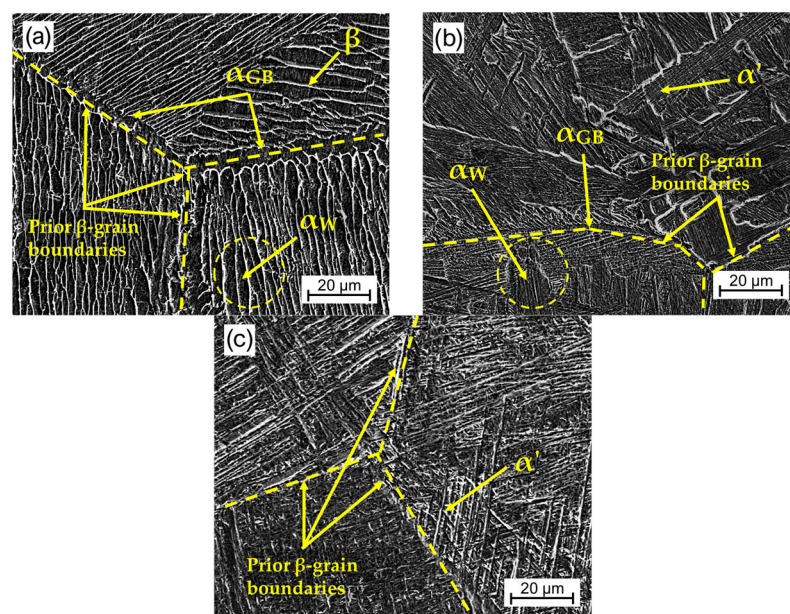


Figure 2. Scanning electron microscope images of Ti-407 alloy after β -anneal heat treatment at 940 °C for 1 h followed by (a) slow furnace cooling, (b) air cooling, and (c) water quenching.

As can be observed in Figure 2a, furnace-cooled samples developed a combination of intragranular α -Widmanstätten laths (α_W) and coarser α -phase lamellae (grain boundary allotriomorphs) which decorate the prior β -grain boundaries. This type of microstructure is similar to that observed in Ti-6Al-4V alloy slowly cooled from the β field. In this case, however, the coarse lamellar microstructure is characterized by the presence of grain boundary α (α_{GB}) and α -Widmanstätten (α_W) platelets that nucleate on the α_{GB} layer and grow inside the β grains, while the β phase is stabilized due to the vanadium enrichment during slow cooling.

On the other hand, Figure 2b shows that the air-cooled microstructure developed a combination of acicular martensite (α'), intergranular α -Widmanstätten laths (α_W), and some prior β -grain boundaries decorated with α_{GB} . These observations indicate that at this intermediate cooling rate, a martensitic transformation could not be reached completely, and some amount of lamellar α nucleated and grew.

Finally, as depicted in Figure 2c, water-quenched specimens showed a predominantly martensitic microstructure, characterized by the presence of intragranular needle-shaped α' , as under this condition, the cooling rate was high enough to effectively hinder the diffusion-controlled mechanism of α -phase lamellar growth. This martensitic transformation has also been reported for other titanium alloys, such as Ti 6-Al-4V [32].

The α/α' lath thickness and primary α content as a function of cooling rate were measured using ImageJ software (Version 1.53k) for image analysis. The results are summarized in Table 2. It can be noted that as the cooling rate increases from furnace cooling to water quenching, the α -lath thickness decreases, indicating that α -lath growth is time-dependent, given that, as the cooling rate decreases, the martensitic transformation changes to a diffusional transformation [33]. Also, the resulting primary α content decreases from 82% to 65% as the cooling rate increases, suggesting that a larger fraction of metastable β phase is retained upon rapid cooling.

Table 2. Primary α thickness and volume fraction obtained upon cooling from 940 °C/1 h in different cooling environments.

	Furnace Cool	Air Cool	Water Quench
α lath thickness (μm)	1.7 ± 0.8	0.6 ± 0.3	0.5 ± 0.2
% primary α	82	70	65

High-temperature compression results for the three starting microstructures using constant crosshead speed at different temperatures were used to assess the flow stress behavior and microstructural evolution of this alloy. True stress–true strain curves were computed from load and displacement values gathered from the universal testing machine data acquisition software. Figure 3 shows the flow stress curves up to a true strain of -0.8 .

In general, all samples that were deformed at low temperatures (below 830 °C) exhibited, first, an increase in the flow stress at $0 < \epsilon < 0.1$, resulting from work hardening up to the peak stress, followed by a flow softening until reaching a steady state flow. It is noteworthy that for strains larger than ~ 0.5 , the stress–strain curves exhibit an apparent increase in stress which is associated with the effects of friction during the uniaxial compression tests. This effect is more relevant for test temperatures lower than 850 °C.

The observed work hardening at the initial deformation stage has been reported as well for Ti-6Al-4V alloy with initial lamellar microstructure under high-temperature uniaxial compression below the β -transus temperature [34]. On the other hand, flow softening has been reported in other titanium alloys, and it may be caused by different physical processes, including deformation heating, dynamic globularization of the prior lamellar α laths, kinking of α , shear band formation, and texture change [28]. A similar flow softening behavior is reported for Ti-6Al-4V alloy as a result of the globularization of the lamellar structure, that is, the partition of α laths into equiaxed α globules, as well as the progressive realignment of the α laths perpendicular to the loading direction [35,36]. Also, this flow

softening could be attributed to a dynamic transformation of the microstructure, as it has been reported as one of the primary sources of flow softening during the thermomechanical processing of titanium alloys [37].

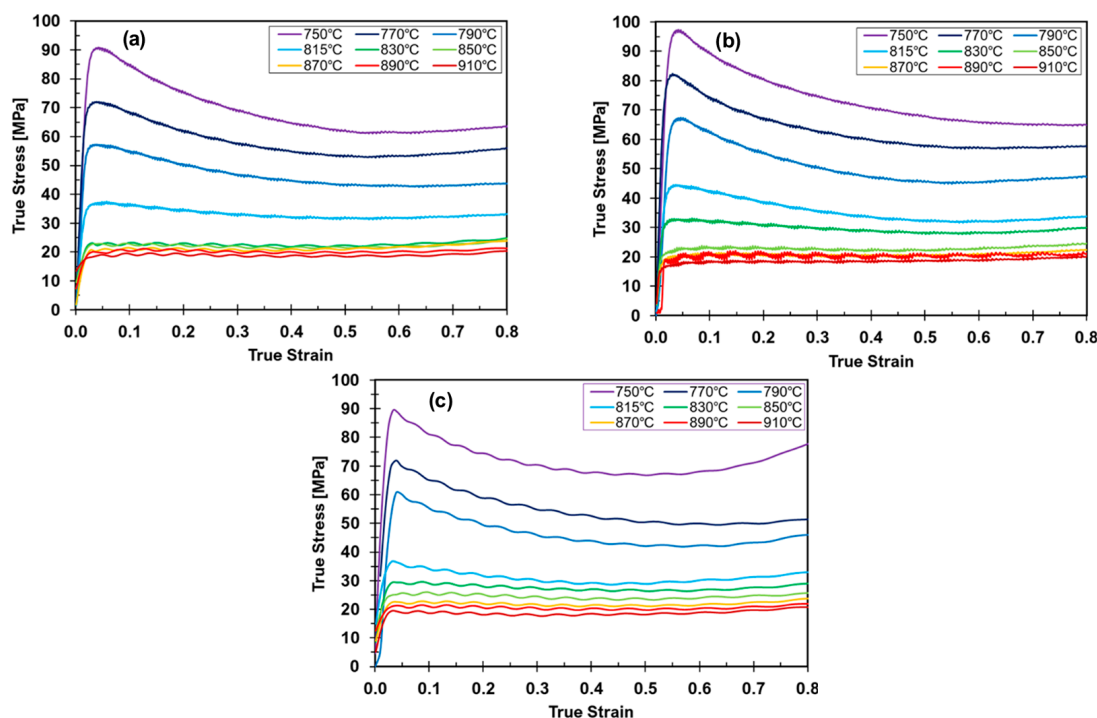


Figure 3. True stress–true strain curves of Ti-407 alloy at constant crosshead speed of 0.05 mm/s up to a deformation $\epsilon = -0.8$ at different temperatures for three initial conditions: (a) β -annealed and slowly cooled in furnace, (b) β -annealed and air-cooled, and (c) β -annealed and water-quenched.

Finally, it was observed that there was an increase in the flow stress at $\epsilon > 0.5$ due to the intensification of frictional forces between the specimen and the compression anvils. For test temperatures $T > 830$ °C, the peak stress and the yield strength were very close to each other, and the flow stress went into a steady state upon reaching the peak stress, indicating the prevalence of dynamic recovery throughout the test.

Regarding the effect of cooling media after β annealing of compression specimens on the yield strength and the peak stress (Figure 4), furnace-cooled samples showed the lowest yield strength, while water-quenched and air-cooled specimens displayed the highest yield strengths, indicating an inverse proportion of mechanical strength with initial α -lath thickness. This behavior is observed especially at the lower deformation temperatures (up to 830 °C). Above this threshold, the influence of initial microstructure on mechanical strength is virtually negligible, as the initial lamellar hcp α phase is increasingly transforming into the high-temperature bcc β phase. This behavior is also reported for Ti-55 near α -titanium alloy as temperature approaches $T_{\beta t}$ [38].

As can be observed in Figure 4, there is a sharp change in the slope of the linear temperature dependence of the yield strength and the peak stress in the temperature range of 830–850 °C. This behavior can be attributed to the $\alpha + \beta \rightarrow \beta$ transformation, which was confirmed by metallographic examination of the deformed samples as discussed below.

Figure 5 shows a reconstruction of optical microscopy images from the cross-section of a compression specimen deformed to a strain of -0.8 at 750 °C. Metallographic analysis revealed different zones within the specimens, characterized by (a) the presence of a heavily worked microstructure in the center of the sample, where strain was mainly concentrated; (b) a dead metal zone in the vicinity of the surfaces as a result of frictional forces due to the contact with the anvils; and (c) a moderately deformed area concentrated in the periphery,

where a barrel shape is formed also as a consequence of friction. At this scale, all samples showed a similar behavior.

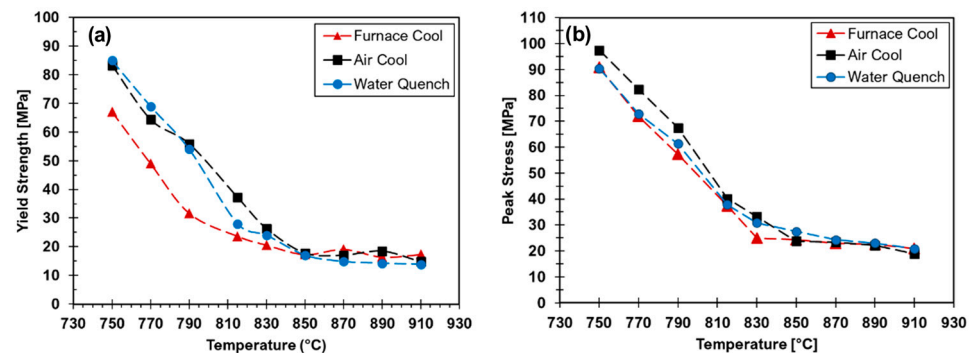


Figure 4. Effect of cooling media after β annealing on compressive yield strength (a) and peak stresses (b) at different temperatures.



Figure 5. Cross-section view of a β -annealed (940 °C/1 h/furnace cool) sample, reheated at 750 °C for 30 min, uniaxially deformed in compression ($\epsilon = -0.8$), and then prepared metallographically to highlight the deformation zones.

To gain more insight into the microstructural evolution of the deformed samples, higher magnification optical microscopy images from the center (intense shearing zone) of the specimens are presented in Figures 6–8 for the three different starting conditions. In addition, the lower left corner of each of these pictures shows a higher magnification SEM image.

At a low deformation temperature (750 °C), plastic deformation causes coarsening and realignment of elongated α grains in the direction normal to the applied stress, independently of the initial microstructure (compare Figures 6a, 7a and 8a).

As the deformation temperature increases to 790 °C, coarsening of the elongated α grains occurs faster, and an alignment perpendicular to the compression axis is also evident in the material that was furnace-cooled after the β -annealing treatment (Figure 6b). In contrast, in deformed air-cooled and water-quenched specimens, the α laths become kinked, as depicted in Figures 7b and 8b.

Compressive deformation at 830 °C and higher temperatures causes drastic changes in the microstructure. As can be seen in Figures 6c and 8c, after deformation at 830 °C, material furnace-cooled or water-quenched after the β -annealing treatment exhibits the presence of equiaxed α grains within a transformed β matrix, which indicates that this temperature is just below the $T_{\beta t}$. A similar behavior has been reported for titanium alloy TA15, in which the deformation above a critical globularization strain [39] at temperatures close to $T_{\beta t}$ influenced the volume fraction and aspect ratio of the α phase [40]. On the other hand,

the sample that was air-cooled after the β annealing (Figure 7c) exhibits a microstructure consisting of a combination of elongated and equiaxed α grains in a transformed β matrix.

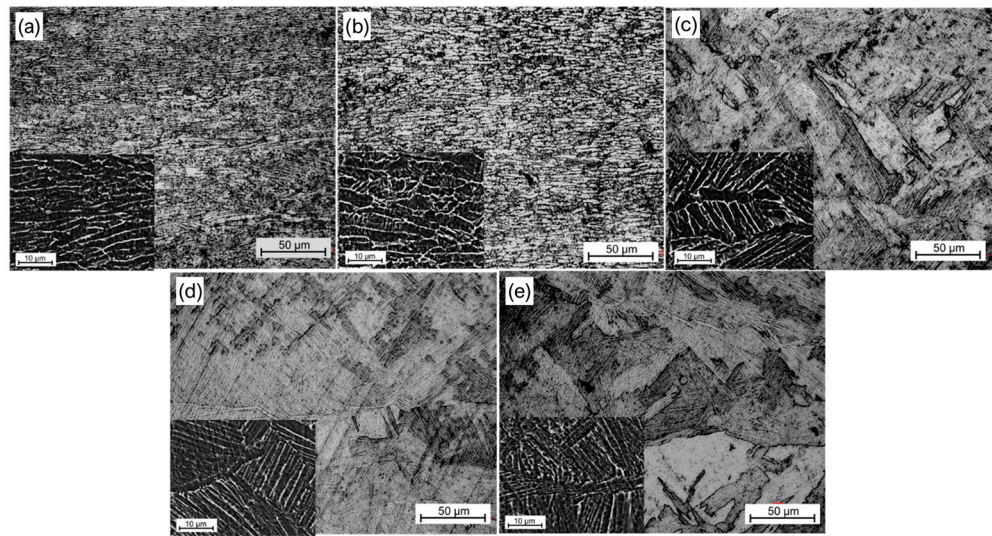


Figure 6. Microstructure of Ti-407 alloy after β annealing at 940 °C/1 h, furnace cooling, and subsequent uniaxial compression ($\epsilon = -0.8$) at 0.05 mm/s at different temperatures: 750 °C (a), 790 °C (b), 830 °C (c), 870 °C (d), and 910 °C (e).

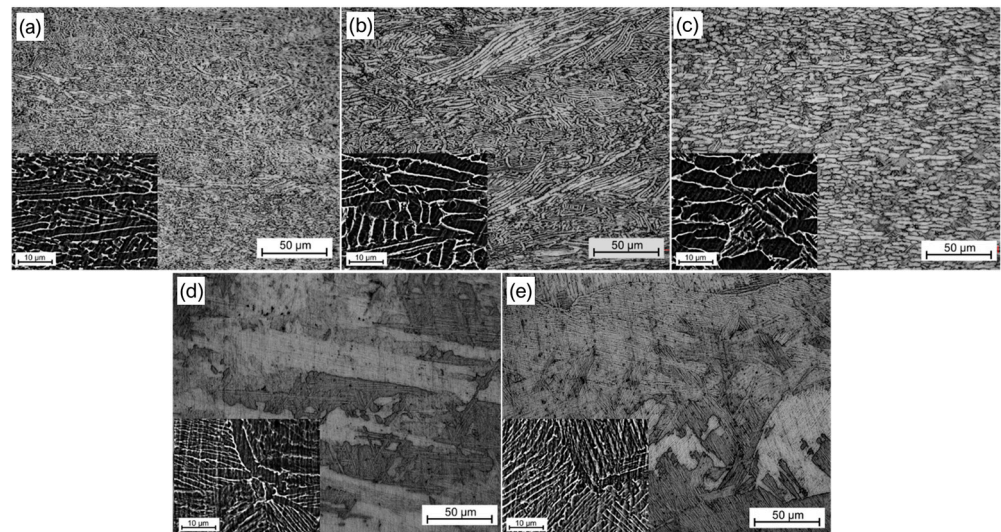


Figure 7. Microstructure of Ti-407 alloy after β annealing at 940 °C/1 h, air cooling, and subsequent uniaxial compression ($\epsilon = -0.8$) at 0.05 mm/s at different temperatures: 750 °C (a), 790 °C (b), 830 °C (c), 870 °C (d), and 910 °C (e).

Upon plastic deformation at $T > 850$ °C, coarse β grains containing intragranular lamellar α were identified in the deformed samples (Figure 6d,e, Figure 7d,e and Figure 8d,e), confirming that deformation was carried out above the $T_{\beta t}$, and α laths were observed to be nucleated during the cooling stage after compression. Even with the high strain magnitude applied ($\epsilon = -0.8$), at this temperature, globularization of the α phase was not achieved, as there was no α phase present during high-temperature deformation.

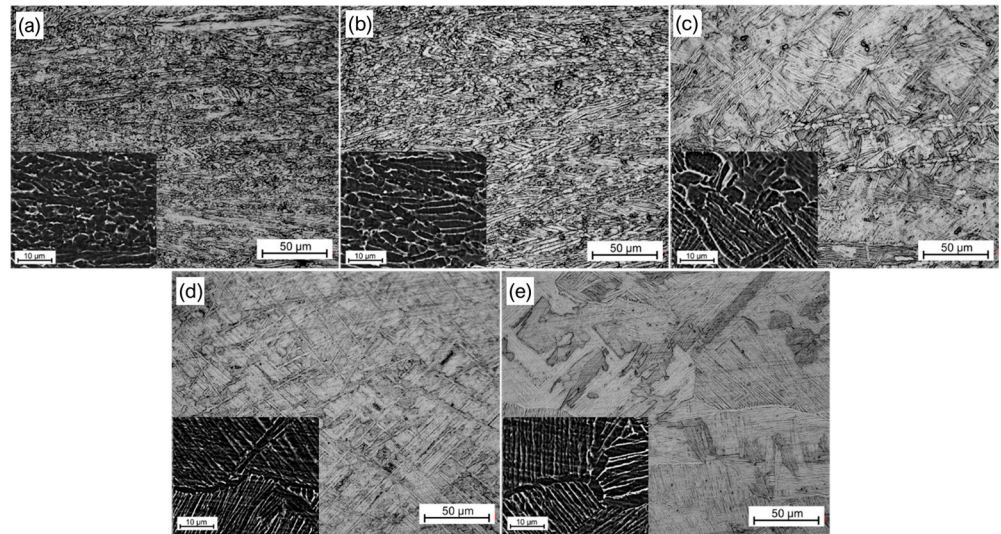


Figure 8. Microstructure of Ti-407 alloy after β annealing at 940 °C/1 h, water quenching, and subsequent uniaxial compression ($\epsilon = -0.8$) at 0.05 mm/s at different temperatures: 750 °C (a), 790 °C (b), 830 °C (c), 870 °C (d), and 910 °C (e).

Comparing the initial microstructure presented in Figure 2a–c with the deformation microstructures presented in Figures 6–8, respectively, it becomes evident that plastic deformation in uniaxial compression at $T < 790$ °C produces elongated and kinked α laths. As the temperature increases above 790 °C but below $T_{\beta t}$, the elongated and kinked α laths suffer a change in morphology to globular α grains with aspect ratios < 3 . A similar transformation of the α phase towards an equiaxed morphology upon high-temperature deformation close to $T_{\beta t}$ has also been reported for Ti-6Al-4V and Ti-6Al-2Mo-2V-1Fe, as a result of spheroidization [41–43]. Finally, for deformation at $T > T_{\beta t}$, the α phase observed after cooling to room temperature exhibits a lamellar morphology, regardless of the magnitude of the strain ($\epsilon = -0.8$) applied during uniaxial compression testing.

The globular α fraction, measured as an area percentage on SEM images with ImageJ software, increased with testing temperature (Figure 9), indicating that the globularization process is highly dependent on temperature. This temperature dependence has been reported as well for Ti60 alloy (Ti-5.6Al-3.7Sn-3.2Zr-0.5Mo-0.4Nb-1.0Ta-0.37Si-0.05C), also influencing the crystallographic orientation evolution of both the α and β phases [44]. The maximum globular α fraction was obtained in the range of 815–830 °C, while transformation to the β phase was completed at ~835–870 °C for the three initial conditions. This temperature was estimated from the temperature dependence of the yield strength and the peak stress (Figure 3) and confirmed by non-isothermal dilatometry (Figure 1).

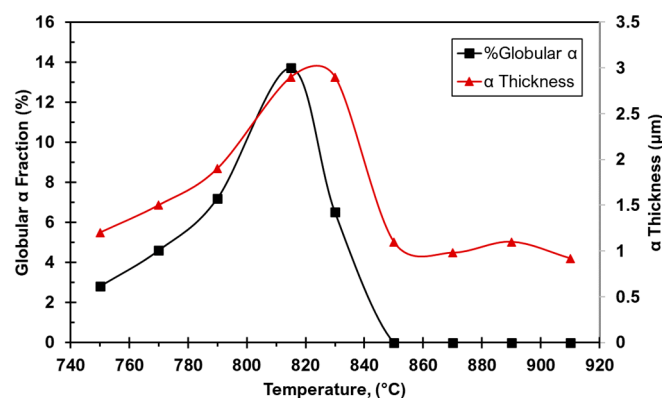


Figure 9. Globular α -phase fraction obtained after β annealing at 940 °C/1 h and cooling in furnace/air/water and subsequent uniaxial compression at different temperatures.

As can be seen in Figure 4, the completion of the $(\alpha + \beta) \rightarrow \beta$ transformation causes a change in the slope of the strength–temperature relationship. On the other hand, the α -phase thickness, also measured with ImageJ software, increased with temperature up to 830 °C. Above this threshold, the α -phase thickness decreases to a minimum and does not change significantly as the deformation temperature increases to 910 °C. This observation suggests that after the plastic deformation of Ti-407 at $T > T_{\beta t}$, α -lath thickness obtained by cooling from the β -phase field is independent of temperature, irrespective of the initial microstructure. This finding correlates well with the plateau in yield and peak stresses shown in Figure 3 for deformation temperatures $T > 835$ °C, shown in Figure 4, evidencing the dependence of mechanical strength on α -lath thickness.

4. Conclusions

The initial microstructure and temperature dependence of the flow stress of Ti-407 alloy was determined using uniaxial compression tests in the range of 750–910 °C. Initial lamellar microstructures with different lath thicknesses were obtained via β annealing at 940 °C for one hour and then furnace cooling, air cooling, or water quenching. The following conclusions are drawn from this investigation:

- (1) Compressive yield strength revealed a marked dependence on the initial microstructure. Yield strengths of furnace-cooled specimens were consistently lower throughout the test temperatures up to about 835 °C, where all initial microstructures converge at a yield strength of 14 MPa. This behavior is attributed to the higher α lath thickness of furnace-cooled specimens (1.7 ± 0.8 μm) in comparison with air-cooled and water-quenched samples (0.6 ± 0.3 μm and 0.5 ± 0.2 μm , respectively), as there are fewer inter-lath β ligaments per unit area to hinder dislocation motion.
- (2) The globular α fraction increased with temperature, reaching a maximum of 15–16% in the range of 815–830 °C, just below the $T_{\beta t}$. Deformation at temperatures below 815 °C produced predominantly elongated α phase, indicating that the strain magnitude solely is not enough to promote globularization of the α phase, but a certain temperature threshold below the $T_{\beta t}$ must be reached.
- (3) Flow stress behavior revealed two temperature-dependent regimes based on the form of the true stress–true strain curves: (a) the low-temperature regime (750–815 °C) showing a peak stress at $\epsilon < 0.1$ as a result of work hardening, followed by a softening stage, characterized by morphological changes in the alpha phase (kinking and then globularization) as well as flow localization, and (b) the high-temperature regime (830–910 °C), where flow stress remains virtually constant after reaching the peak stress, indicating a continuous competition of strain hardening and dynamic recovery in the deformed β grains.

Author Contributions: Conceptualization, A.S.; methodology, E.L., H.G. and A.S.; investigation, L.B.; writing—original draft, L.B.; writing—review and editing, E.L., H.G. and A.S.; supervision, E.L., H.G. and A.S. All authors have read and agreed to the published version of the manuscript.

Funding: This research was funded by FRISA Aerospace, funding ID: SA/SAL/IS/2019/001906, and the APC was funded by CINVESTAV.

Data Availability Statement: The original contributions presented in the study are included in the article, further inquiries can be directed to the corresponding authors.

Acknowledgments: The authors gratefully acknowledge the financial support of FRISA Aerospace as well as UANL and CINVESTAV laboratories for supplying all necessary characterization equipment.

Conflicts of Interest: The authors declare no conflicts of interest.

References

1. Henriques, V.A.R.; de Campos, P.P.; Cairo, C.A.A.; Bressiani, J.C. Production of titanium alloys for advanced aerospace systems by powder metallurgy. *Mater. Res.* **2005**, *8*, 443–446. [\[CrossRef\]](#)
2. Hatt, O.; Lomas, Z.; Thomas, M.; Jackson, M. The effect of titanium alloy chemistry on machining induced tool crater wear characteristics. *Wear* **2018**, *408–409*, 200–207. [\[CrossRef\]](#)
3. James, S.; Kosaka, Y.; Thomas, R.; Garratt, P. TIMETAL 407: A titanium alloy to enable cost reduction. In Proceedings of the 13th World Conference on Titanium, San Diego, CA, USA, 16–20 August 2015; John Wiley & Sons, Inc.: Hoboken, NJ, USA, 2016.
4. Davey, W.; Bache, M.; Davies, H.; Thomas, M. Fatigue performance of the novel titanium alloy Timetal 407. *MATEC Web Conf.* **2018**, *165*, 4001. [\[CrossRef\]](#)
5. Sneddon, S.; Mulvihill, D.M.; Wielewski, E.; Dixon, M.; Rugg, D.; Li, P. Deformation and failure behavior of a titanium alloy Ti-407 with reduced aluminum content: A comparison with Ti-6Al-4V in tension and compression. *Mater. Charact.* **2021**, *172*, 110901. [\[CrossRef\]](#)
6. Truax, D.; McMahon, C. Plastic behavior of titanium-aluminum alloys. *Mater. Sci. Eng.* **1974**, *13*, 125–139. [\[CrossRef\]](#)
7. Kimura, A.; Nakamura, S.; Isogawa, S.; Matsubara, T.; Kimura, K.; Sato, Y. *A Free Machining Titanium Alloy for Connecting Rods*; SAE International: Pittsburgh, PA, USA, 1991.
8. Singh, G.; da Fonseca, J.Q.; Preuss, M. Microstructure evolution and deformation texture during rolling of TIMETAL®407. *Materialia* **2020**, *9*, 100596. [\[CrossRef\]](#)
9. Bache, M.; Davies, H.; Davey, W.; Thomas, M.; Berment-Parr, I. Microstructural control of fatigue behavior in a novel alpha+beta titanium alloy. *Metals* **2019**, *9*, 1200. [\[CrossRef\]](#)
10. Murray, J. Calculation of the titanium-aluminum phase diagram. *Metall. Trans. A* **1988**, *19*, 243–247. [\[CrossRef\]](#)
11. Singh, G.; Souza, P.M. Hot deformation behavior of a novel alpha+beta titanium alloy TIMETAL®407. *J. Alloys Compd.* **2023**, *935*, 1. [\[CrossRef\]](#)
12. Dredge, C.; M'saoubi, R.; Thomas, B.; Hatt, O.; Thomas, M.; Jackson, M. A low-cost machinability approach to accelerate titanium alloy development. *J. Eng. Manuf.* **2021**, *235*, 1618–1632. [\[CrossRef\]](#)
13. Semiatin, S.L.; Seetharaman, V.; Weiss, I. The thermomechanical processing of alpha/beta titanium alloys. *JOM* **1997**, *49*, 33–39. [\[CrossRef\]](#)
14. Seshacharyulu, T.; Medeiros, S.; Frazier, W.; Prasad, Y. Microstructural mechanisms during hot working of commercial grade Ti-6Al-4V with lamellar starting structure. *Mater. Sci. Eng.* **2002**, *325*, 112–125. [\[CrossRef\]](#)
15. Warchomicka, F.; Poletti, C.; Stockinger, M.; Henke, T. Microstructure evolution during hot deformation of Ti-6Al-4V double cone specimens. *Int. J. Mater. Form* **2010**, *3*, 215–218. [\[CrossRef\]](#)
16. Zhang, J.; Li, X.; Xu, D.; Yang, R. Recent progress in the simulation of microstructure evolution in titanium alloys. *Prog. Nat. Sci. Mater. Int.* **2019**, *29*, 295–304. [\[CrossRef\]](#)
17. Sun, J.; Qi, M.; Zhang, J.; Li, X.; Wang, H.; Ma, Y.; Xu, D.; Lei, J.; Yang, R. Formation mechanism of α lamellae during $\beta \rightarrow \alpha$ transformation in polycrystalline dual-phase Ti alloys. *J. Mater. Sci. Technol.* **2021**, *71*, 98–108. [\[CrossRef\]](#)
18. Durodola, J. Machine learning for design, phase transformation and mechanical properties of alloys. *Prog. Mater. Sci.* **2022**, *123*, 100797. [\[CrossRef\]](#)
19. Mueller, T.; Kusne, A.G.; Ramprasad, R. Machine learning in materials science: Recent progress and emerging applications. *Rev. Comput. Chem.* **2016**, *29*, 186–273.
20. Bignon, M.; Bertrand, E.; Rivera-Díaz-Del-Castillo, P.E.; Tancret, F. Martensite formation in titanium alloys: Crystallographic and compositional effects. *J. Alloys Compd.* **2021**, *872*, 159636. [\[CrossRef\]](#)
21. Niu, Y.; Hong, Z.-Q.; Wang, Y.-Q.; Zhu, Y.-C. Machine learning-based beta transus temperature prediction for titanium alloys. *J. Mater. Res. Technol.* **2023**, *23*, 515–529. [\[CrossRef\]](#)
22. Guo, K.; Yang, Z.; Yu, C.-H.; Buehler, M.J. Artificial intelligence and machine learning in design of mechanical materials. *Mater. Horiz.* **2021**, *8*, 1153–1172. [\[CrossRef\]](#)
23. Banerjee, D.; Williams, J.C. Perspectives on titanium science and technology. *Acta Mater.* **2013**, *61*, 844–879. [\[CrossRef\]](#)
24. Wang, X.; Zhan, M.; Gao, P.; Ma, P.; Yang, K.; Lei, Y.; Li, Z. Deformation mode dependent mechanism and kinetics of dynamic recrystallization in hot working of titanium alloy. *Mater. Sci. Eng. A* **2022**, *772*, 138804. [\[CrossRef\]](#)
25. Tarín, P.; Gualo, A.; Simón, A.G.; Piris, N.M.; Badía, J.M. Study of alpha-beta transformation in Ti-6Al-4V-ELI. Mechanical and microstructural characteristics. *Mater. Sci. Forum* **2010**, *638–642*, 712–717. [\[CrossRef\]](#)
26. Ding, C.; Li, X.; Zhu, H.-Y.; Chen, F.-W.; Li, F.; Chang, H. Microstructure evolution and phase transformation kinetics of low cost Ti-35421 titanium alloy during continuous heating. *J. Mater. Res. Technol.* **2021**, *14*, 620–630. [\[CrossRef\]](#)
27. Yu, H.; Li, W.; Zou, H.; Li, S.; Zhai, T.; Liu, L. Study on Non-Isothermal Transformation of Ti-6Al-4V in Solution Heating Stage. *Metals* **2019**, *9*, 968. [\[CrossRef\]](#)
28. Gao, P.; Fu, M.; Zhan, M.; Lei, Z.; Li, Y. Deformation behavior and microstructure evolution of titanium alloys with lamellar microstructure in hot working process: A review. *J. Mater. Sci. Technol.* **2020**, *39*, 56–73. [\[CrossRef\]](#)
29. Park, C.; Won, J.W.; Park, J.-W.; Semiatin, S.L.; Lee, C.S. Mechanisms and kinetics of static spheroidization of hot-worked Ti-6Al-2Sn-4Zr-2Mo-0.1Si with a lamellar microstructure. *Metall. Mater. Trans. A* **2012**, *43*, 977–985. [\[CrossRef\]](#)
30. Lindwall, G.; Wang, P.; Kattner, U.R.; Campbell, C.E. The effect of oxygen on phase equilibria in the Ti-V system: Impacts on the AM processing of Ti alloys. *J. Mater.* **2018**, *70*, 1692–1705. [\[CrossRef\]](#)

31. Joshi, V.A. *Titanium Alloys: An Atlas of Structures and Fracture Features*; CRC Press: Boca Raton, FL, USA, 2006.
32. Feng, Z.; Yang, Y.; Xu, Z.; Shi, Q. Effect of martensitic transformation on elastic modulus anisotropy of Ti-6Al-4V alloy. *Mater. Res.* **2018**, *21*, 1–8. [[CrossRef](#)]
33. Feng, S.; Jinshan, L.; Hongchao, K.; Wenzhong, L.; Xianghong, L.; Yong, F. Phase transformation during the continuous cooling in near alpha titanium alloy Ti60. *Rare Met. Mater. Eng.* **2015**, *44*, 848–853. [[CrossRef](#)]
34. Zhang, W.; Ding, H.; Zhao, J.; Yang, B.; Yang, W. Hot deformation behavior and processing maps of Ti-6Al-4V alloy with starting fully lamellar structure. *J. Mater. Res.* **2018**, *33*, 3677–3688. [[CrossRef](#)]
35. Perumal, B.; Rist, M.A.; Gungor, S.; Brooks, J.W.; Fitzpatrick, M.E. The effect of hot deformation parameters on microstructure evolution of the alpha-phase in Ti-6Al-4V. *Metall. Mater. Trans. A* **2016**, *47*, 4128–4136. [[CrossRef](#)]
36. Zhang, J.; Li, H.; Zhan, M. Review on globularization of titanium alloy with lamellar colony. *Manufacturing* **2020**, *7*, 18. [[CrossRef](#)]
37. Guo, B.; Liu, Y.; Jonas, J.J. Dynamic transformation of two-phase titanium alloys in stable and unstable states. *Metall. Mater. Trans. A* **2019**, *50*, 4502–4505. [[CrossRef](#)]
38. Wu, F.; Xu, W.; Jin, X.; Zhong, X.; Wan, X.; Shan, D.; Guo, B. Study on hot deformation behavior and microstructure evolution of Ti-55 high temperature titanium alloy. *Metals* **2017**, *7*, 319. [[CrossRef](#)]
39. Wang, L.; Fan, X.; Zhan, M.; Jiang, X.; Liang, Y.; Zheng, H.; Liang, W. Revisiting the lamellar globularization behavior of a two-phase titanium from the perspective of deformation modes. *J. Mater. Process. Technol.* **2021**, *289*, 116963. [[CrossRef](#)]
40. Ji, R.; Zhu, K.; Zhang, H.; Luo, H.; Mao, J. Microstructure evolution, mechanical response and strengthening models for TA15 titanium alloy during thermal processes: A brief review. *J. Mater. Res. Technol.* **2024**, *28*, 1644–1656. [[CrossRef](#)]
41. Yan, Z.; Liu, H.; Dai, X.; Li, L.; Zhang, Z.; Wang, Q.; Xue, Y. Effect of multi-pass cooling compression and subsequent heat treatment on microstructural and mechanical evolution of TC4 alloys. *J. Mater. Res. Technol.* **2023**, *23*, 3137–3150. [[CrossRef](#)]
42. Ge, J.; Zhan, X.; Li, C.; Zhang, X.; Zhou, K. Dynamic spheroidization mechanism and its orientation dependence of Ti-6Al-2Mo-2V-1Fe alloy during subtransus hot deformation. *Materials* **2023**, *16*, 5752. [[CrossRef](#)]
43. Aguirre, J.; Erice, B.; Arrese, P.; Otegi, N.; Galdos, L. Effect of near beta-transus forging parameters on the mechanical and microstructural properties of Ti-6Al-4V—Application to hammer forging. *Mater. Res. Proc.* **2023**, *28*, 675–682.
44. Zhao, Z.; Zhang, B.H.; Sun, H.; Wang, Q.J.; Liu, J.R.; Yang, R. Influence of globularization process on local texture evolution of a near- α titanium alloy with a transformed microstructure. *Metall. Mater. Trans. A* **2023**, *54*, 2849–2857. [[CrossRef](#)]

Disclaimer/Publisher’s Note: The statements, opinions and data contained in all publications are solely those of the individual author(s) and contributor(s) and not of MDPI and/or the editor(s). MDPI and/or the editor(s) disclaim responsibility for any injury to people or property resulting from any ideas, methods, instructions or products referred to in the content.